View metadata, citation and similar papers at core.ac.uk

brought to you by CORE

provided by Elsevier - Publisher Connector

Journal of Saudi Chemical Society (2017) **21**, 238–244

King Saud University

Journal of Saudi Chemical Society

www.ksu.edu.sa
www.sciencedirect.com

ORIGINAL ARTICLE

Self-organization of nickel nanoparticles dispersed in acetone: From separate nanoparticles to three-dimensional superstructures

I. Hernández-Pérez [a], L. Díaz Barriga-Arceo [b], V. Garibay Febles [c], R. Suárez-Parra [d], R. Luna Paz [a], Patricia Santiago [e], Luis Rendón [e], José Acosta Jara [f], J.C. Espinoza Tapia [a], L. González-Reyes [a,*]

[a] *Universidad Autónoma Metropolitana-A, Departamento de Ciencias Básicas, Av. Sn. Pablo No. 180, México 02200, D.F., Mexico*
[b] *Instituto Politécnico Nacional, Departamento de Ingeniería Metalúrgica y Materiales, ESIQIE-UPALM, México, D.F. 07738, Mexico*
[c] *Instituto Mexicano del Petróleo, Eje Central Lázaro Cárdenas Norte 152 Col. San Bartolo Atepehuacan, México, D.F. C.P 07730, Mexico*
[d] *Instituto de Energías Renovables, IER-UNAM, Priv. Xochicalco S/N, Temixco, Morelos 62580, Mexico*
[e] *Instituto de Física, Universidad Nacional Autónoma de, México, D.F. México, Mexico*
[f] *Universidad ESAN, Alonso de Molina 1652 Monterrico, Surco, Lima, Peru*

Received 30 May 2016; revised 2 September 2016; accepted 5 September 2016
Available online 14 September 2016

KEYWORDS

Self-organization;
Nickel nanoparticles;
Three-dimensional superstructures;
Sonochemistry

Abstract Sonochemical synthesis of monodisperse nickel nanoparticles (Ni-NPs) by reduction of Ni acetylacetonate in the presence of polyvinylpyrrolidone stabilizer is reported. The Ni-NPs size is readily controlled to 5 nanometer diameter with a standard deviation of less than 5%. The as-prepared Ni-NPs sample was dispersed in acetone, for 4 weeks. For structural analysis was not applied to a magnetic field or heat treatment as key methods to direct the assembly. The transition from separate Ni-NPs into self-organization of three dimensions (3D) superstructures was studied by electron microscopy. Experimental analysis suggests that the translation and rotation movement of the Ni-NPs are governed by magnetic frustration which promotes the formation of different geometric arrangements in two dimensions (2D). The formation of 3D superstructures is confirmed from scanning electron microscopy revealing a layered domain that consists of staking of several

* Corresponding author.
E-mail address: lgr@correo.azc.uam.mx (L. González-Reyes).
Peer review under responsibility of King Saud University.

ELSEVIER Production and hosting by Elsevier

http://dx.doi.org/10.1016/j.jscs.2016.09.001
1319-6103 © 2016 King Saud University. Production and hosting by Elsevier B.V.
This is an open access article under the CC BY-NC-ND license (http://creativecommons.org/licenses/by-nc-nd/4.0/).

monolayers having multiple well-defined supercrystalline domains, enabling their use for optical, electronic and sensor applications.

© 2016 King Saud University. Production and hosting by Elsevier B.V. This is an open access article under the CC BY-NC-ND license (http://creativecommons.org/licenses/by-nc-nd/4.0/).

1. Introduction

The organization and self-assembly of nanostructured materials with controlled size and composition are fundamental with a technological interest over recent years. These kinds of materials provide the critical building blocks for nanoscience and nanotechnology exhibiting new and enhanced properties compared to bulk materials. The effort to understand the physical properties of ever smaller structures has been paralleled by attempts to exploit their beneficial properties. Indeed, in the field of magnetic particles, physical parameters defined as constants in descriptions of bulk materials properties, become size dependent [1]. In other words, changing the size and shape of nanoscale materials produces new materials. Furthermore, the self-assembly of magnetic nanoparticles can lead to superstructures with important collective properties such as data store device [2], spin-dependent electron transport [3], photonic crystals [4], tandem catalysis [5], and a rich variety of novel phenomena derived from their collective interactions.

In this context, the self-assembly of Ni-NPs into three dimensional (3D) superstructures arouse intensive interests from the perspective of both fundamental research and application purpose. Reports on the preparation of Ni nanoparticles self-assembly are not common compared to numerous reports on the preparation of 3D superstructures such as CdSe [6,7], Au [8–10], Ag [11–13], and Co [14,15]. Also, the development of synthetic routes has been employed to synthesize Ni nanoparticles in both organic and aqueous media [16–18] and surfactants are generally used to synthesize monodispersed Ni-NPs [19–22]. However, very limited information is available on the transition from separate Ni-NPs to self-organization in aggregates at a microscopic scale. Therefore, the present study focuses on the synthesis of Ni-NPs with tunable sizes using a simple sonochemistry synthesis in the presence of polyvinylpyrrolidone (PVP) stabilizer. The as-prepared sample was dispersed in acetone and the interplay between crystallographic ordering and its dynamics were discussed herein.

2. Experimental

2.1. Reagents and materials

All chemicals used in this experiment were of reagent grade. Ni $(OCOCH_3)_2 \cdot 4H_2O$ ($\geqslant$98%, Aldrich) was used as nickel source, acetone ($\geqslant$99.9%, Aldrich), isopropyl alcohol ($\geqslant$99.7%, Aldrich) and Poly(vinyl pyrrolidone, PVP, M_w = 40,000) were used as received without further purification. The water used throughout this work was deionized water.

2.2. Synthesis of nickel nanoparticles

Nickel nanoparticles were synthesized as follows: 1 g of Ni $(OCOCH_3)_2 \cdot 4H_2O$ was dissolved in a mixture of 10 mL of acetone and 10 mL of Isopropyl alcohol. The reaction mixture was exposed to ultrasound irradiation (20 Khz) for 20 min. At this time, 0.05 g of PVP was added to the mix and the ultrasonic treatment extended until 50 min [23] was completed. The reaction formed a black solid, which was separated by centrifugation and washed several times with acetone and isopropyl alcohol and dried at room temperature. The as-prepared sample was redispersed in 15 mL of acetone. The suspension of Ni-NPs was preserved inside a vertically positioned glass vial for a maximum time of 4 weeks. After this time, five samples were obtained and they are identified by its week number (as-prepared, W1, W2, W3 and W4) along this paper. It is important to remark that no heat treatment was implemented after the sonochemical synthesis of Ni-NPs in order to preserve the crystalline structure and the crystal size of the as-prepared sample.

2.3. Characterization

X-ray diffraction (XRD) patterns were carried out with a Bruker X-ray diffractometer D8 Focus (λ = 1.5406 Å) with 35 kV and 25 mA. High resolution transmission electron microscopy (HRTEM) and a scanning transmission electron microscope (STEM) operated in the mode in which the scattered electrons are collected by means of a high-angle annular dark-field (HAADF) detector to provide the critical experimental input needed to determine the full-structure evolution of the assembled Ni-NPs. Therefore, the morphology and structure were characterized on a Tecnai F30 (Cs = 1.2 nm) operated at an accelerating voltage at 300 kV having a point-to-point resolution of 0.20 nm and lattice resolution of 0.14 nm. Samples for HRTEM and STEM crystallographic analyses were prepared by evaporation of one drop of Ni-NPs solution on carbon-coated copper grids (300 mesh) and then dried under air. Morphological evolution analysis was conducted on a scanning electron microscopy (SEM, FEI-Nova 200 Nanolab) operated at 10 kV.

3. Results and discussion

The corresponding XRD spectrum for the as-prepared sample (Fig. 1) clearly shows the presence of a single face-centered cubic (FCC) crystal phase of Ni NPs with only three reflections, (2θ = 44.6°, 51.84° and 76.48°), corresponding to Miller indices (1 1 1), (2 0 0) and (2 2 0) respectively (JCPDS 04-0850). No peaks of nickel oxide were detected within the XRD analysis limit, indicating that pure FCC nickel was obtained under such experimental conditions. The nanometric crystallite size can easily be detected by the broadening of the (1 1 1) reflection, due to that the XRD reflections are usually inversely correlated with the crystallite diameter of the particles. The size of coherently diffracting domains was calculated by considering the size broadening contribution only and to determine the grain size based on the (1 1 1) reflection the Debye-Scherrer

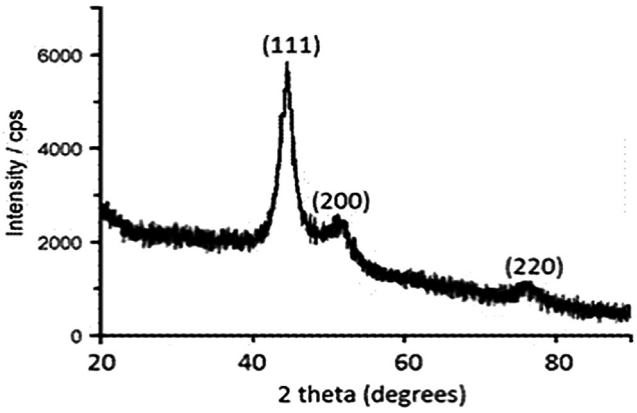

Figure 1 XRD pattern of the as-prepared Ni-NPs.

equation was used: $D = 0.9\lambda/\beta\cos\theta$, where D is the average diameter of the calculated particles, λ is the wave length characteristic in Å (in this particular case λ = 1.5405 Å), β is the full width at half maximum and θ is Bragg's angle [24]. Therefore, the crystalline grain size calculated from the XRD pattern according to the Debye–Scherrer formula was 5.3 nm.

Low-magnification TEM image reveals that the resulting as-prepared Ni-NPs have a monodisperse size distribution with a standard deviation of less than 5%, and is nearly spherical in shape, Fig. 2A. This result suggests that large isotropic van der Waals interactions induce the formation of spherical and isotropic aggregates [25] in the absence of dipolar interactions. Likewise, faceting morphology can be seen in some particles. Therefore, both shapes, spherical and cubes, correspond to thermodynamically stable geometries. In Fig. 2b, it is confirmed that the particles are single crystals showing the (1 1 1) lattice plane of Ni-FCC with the fringe spacing of 2.07 Å. These results indicate that the shape of Ni-NPs can be controlled in the presence of PVP, which is adsorbed on the Ni-NPs surface and prevents the grain growth. From our structural analysis, the HRTEM images of other particles also show a single-crystal structure.

As it was already mentioned, the samples were labeled as W1, W2, W3, and W4, where W represents the time (in weeks) when the sample was analyzed after the sonochemical synthesis. Representative HAADF image of Ni-NPs corresponding to W1, is shown in Fig. 3a. An arrangement of flexible chains and closed like-rings are observed in a suspension aged for W1. It was understood that due to the magnetic dipolar interactions, one self-assembly is rather typical for magnetic nanoparticles. Such nanoparticles with a magnetic dipole moment should be able to minimize the magnetostatic energy via self-assembly into flexible chains. Close examination of Fig. 3a reveals the organization of Ni-NPs consisting of hexagonally close-packed structures, highlighted with a circle. In order to elucidate this behavior a HRTEM image was analyzed, Fig. 3b. In the central HRTEM image it can be observed that a 5 nm Nickel nanocrystal is surrounded with a hexagon formed by other Ni-NPs, with approximately the same size, 5 nm. The Fast Fourier Transform (FFT) of each particle, enumerated from 1 to 6, shows (200) ($0\bar{2}0$) and ($0\bar{2}\bar{2}$) reflections corresponding only to the FCC Ni phase. Certainly, it is possible to consider that the orientation for a magnetic single-domain is linked to the zone axis and that the magnetic orientation is not the same and also has a certain precession of the magnetic moment.

This magnetic condition allows Ni-NPs to form a metastable arrangement, since there is not a preferential orientation of the axes or zone magnetic moments of the Ni-NPs and apparently the precession of the magnetic moment is given about the same crystallographic plane. This phenomenon is known as magnetic frustration. Magnetic frustration governs movement dynamics of this system particles and promotes the formation of different geometric arrangements of Ni-NPs in 2D [26–33].

Furthermore, a strong tendency and oriented aggregation that self-assembly in fine arrays is clearly observed in Fig. 3a. Therefore, unpaired dipoles present at the ends of a linear chain of nanoparticles can be paired, yielding closed rings, as in the sample W1, shown in Fig. 3a–b. Also, a strong tendency to oriented aggregation in fine self-assembled arrays (as can see

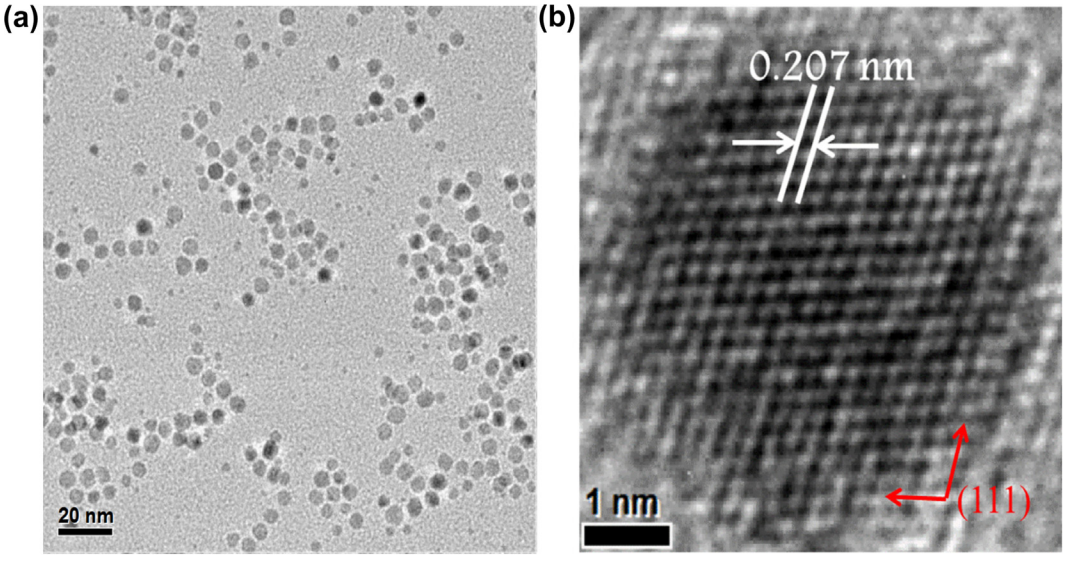

Figure 2 TEM image of (a) as-prepared sample. (b) HRTEM image showing a single crystal structure corresponding to Ni-FCC.

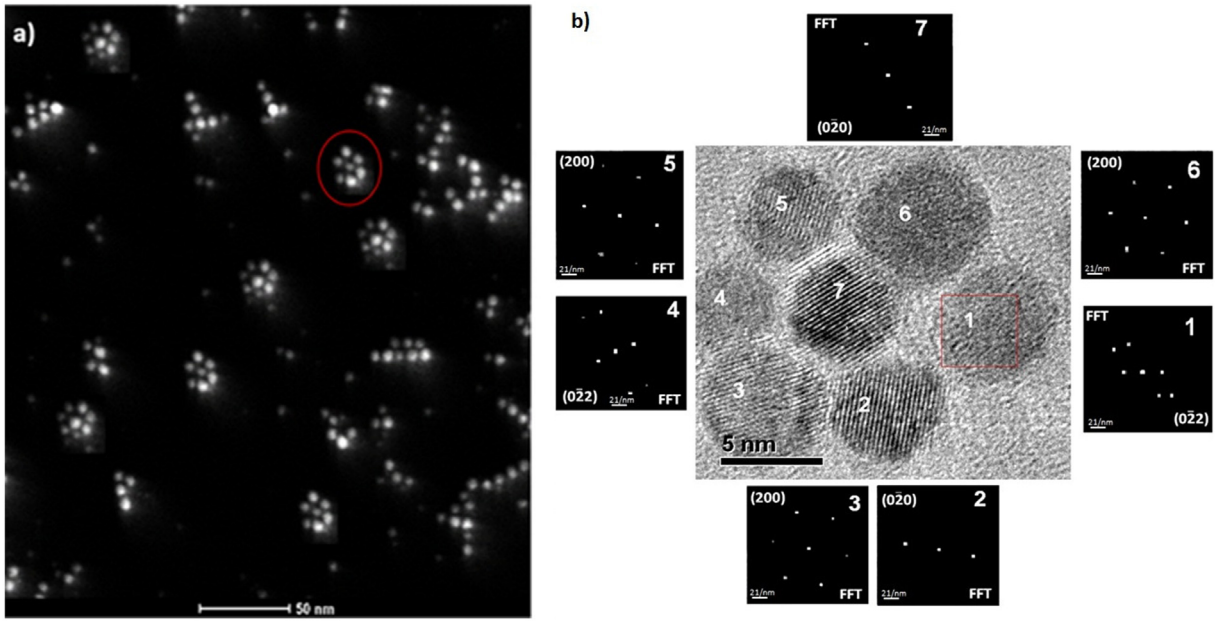

Figure 3 (a) HAADF image corresponding to W1 sample. (b) HRTEM image of hexagonally close-packed structures and FTT analysis of each Ni-NPs.

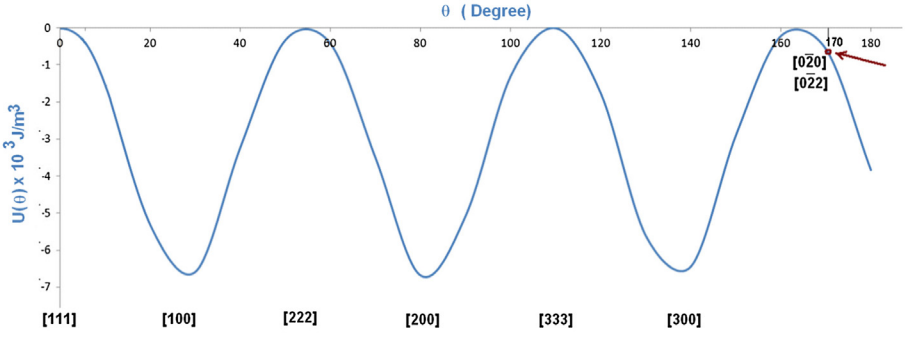

Figure 4 Magnetic anisotropy of nickel nanoparticles as a function of the crystal directions.

in Fig. 3b.) was clearly observed This behavior could be attributed to isotropic van der Waals forces and anisotropic dipole–dipole interactions [34].

In addition, when nanoparticles of magnetic materials are out of the influence of an external field, their crystal relative orientations depend on an unexpected spontaneous magnetization, which is called magnetic anisotropy [35]. Specifically, in the case of Nickel it is known that difficult magnetization axes are parallel to [1 0 0] and the easy magnetization axes are parallel to [1 1 1]. Therefore, is clear to assume that most magnetization is reached in directions parallel to [1 1 1] while the minimum magnetization directions are parallel to [1 0 0].

In a nanoparticles, where the crystal anisotropy is presented about an axis, the energy u_α management function is represented by the angle θ orientation as follows:

$$u_a = \sum_n K_{un} \mathrm{sen}^{2n}\theta$$

where K_{un} are the energies where the maximum magnetization occurs depending on the direction [35].

In nanometric structures, considered as uniaxial domains, only the terms $n = 1$ and $n = 2$ are used, so that magnetization energy is:

$$U = K_1 \mathrm{sen}^2\theta + K_2 \mathrm{Sen}^4\theta$$

In the case of nickel, experimentally was found that $K_1 = -4.5 \times 103\ \mathrm{J/m^3}$ and $K_2 = -2.3 \times 103\ \mathrm{J/m^3}$. Thus, the magnetic anisotropy of nickel shows the variations depicted in the Fig. 4.

In Fig. 4, the U_a shows some maxima and minima as a function of the crystal directions [1 1 1] and [1 0 0] and its multiples. The directions of nickel nanostructures in the samples observed by electron microscopy, Fig. 3b, also indicate the directions [0 2 0] and [0 2 2]. Moreover, the calculated angle for the direction [2 0 0] was located near to 170°, although its energy level does not corresponds, in this case, to the maximum. This fact confirms that Ni-NPs have unstable equilibrium.

In Fig. 5a, corresponding to W2, can be observed the progressive increase in the aggregates of Ni-NPs, forming

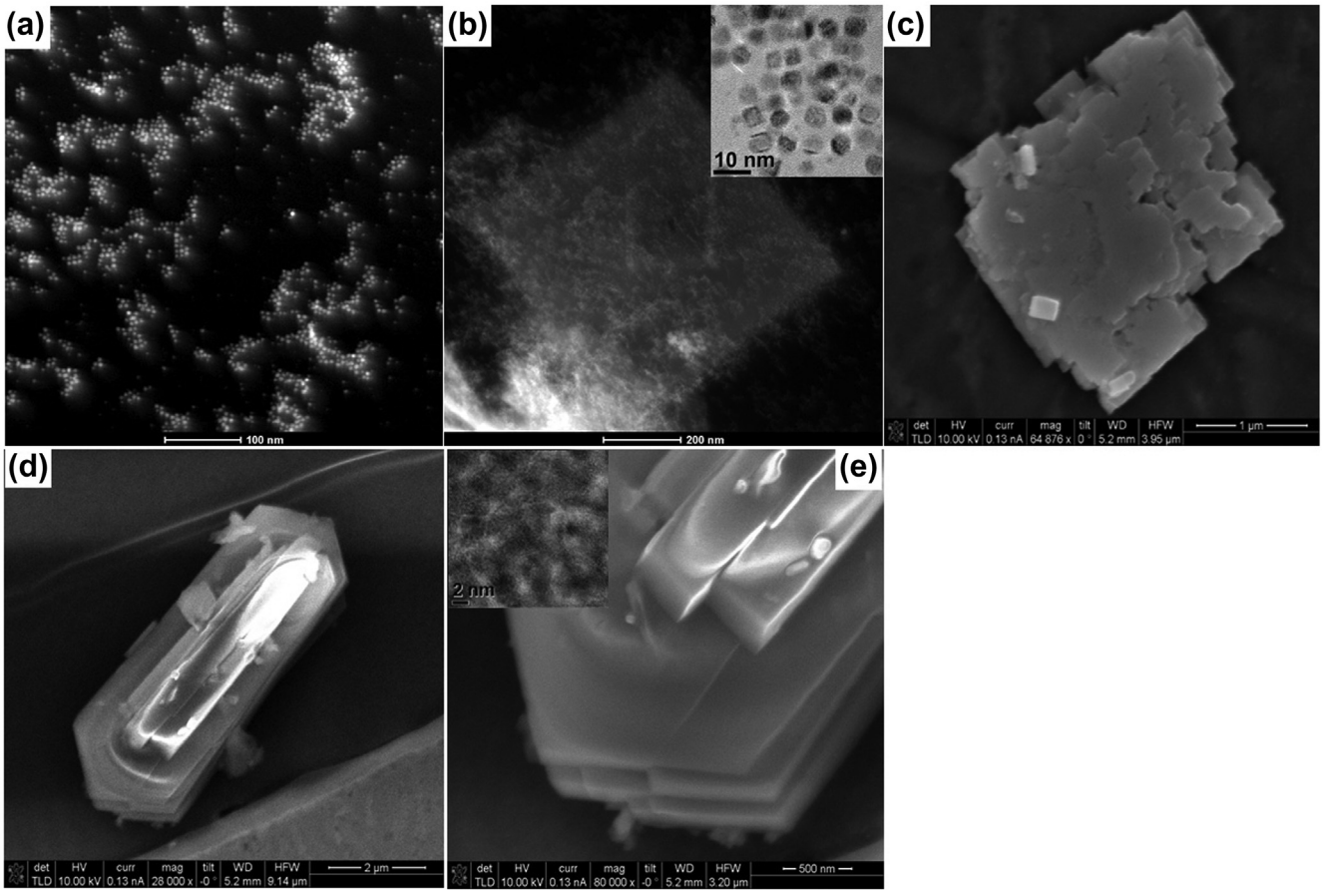

Figure 5 (a) HAADF image corresponding to W2 sample. Is possible observed the progressive increase in the aggregates of Ni-NPs, (b) HAADF image corresponding to W3, Ni-NPs are arranged in a nearly 2D superstructure, and HRTEM reveals that Ni-NPs become more faceted upper inside. (c) HRSEM image shows a layered domain that consists of stacking of several monolayers. (d) Typical overhead view of the sample W4 shows a HRSEM image of a closed packed multilayer 3D. (e) HRSEM image shows the growth of terraces.

branched chains, which can be explained as a cooperative effect of the attractive magnetic interaction between Ni-NPs. Also, these geometrical arrangements are only possible if the particles are mobile enough and have time to find their lowest energy sites. This effect cooperative is more evident in Fig. 5b, corresponding to W3, where the Ni-NPs are arranged in a nearly 2D superstructure, exhibiting long-range order and the self-assembly increased gradually and the dispersity becomes lower and 2D superstructure is formed. However, HRTEM reveals that the particles become more faceted for W3, displaying sharp edges, Fig. 5b upper inset. This morphological change can be attributed to digestive ripening, which does not affect their size but promotes the intraparticular reorganization of nickel atoms [36]. A two-dimensional superstructure preferably grows with facets reflecting the packing symmetry inherent for the Ni-NPs. Moreover, the self-assembly of 2D of Ni-NPs superstructure shows a layered domain, 2D sheets, that consists of stacking of several monolayers are clearly observed in HRSEM image, Fig. 5d. In this case, if the growth conditions are constant, the stacking of monolayers remains the same for the successive formation of new stacking layers.

When the suspension was aged 4 weeks, W4, the thickness of the stacking of monolayers increased up to 0.7 μm, Fig. 5d. Also it was noticed from Fig. 4e that the 3D superstructure is well-faceted and low energy surface facets, such as the {1 1 1} surface facet indicated in Fig. 5e inset, are distinguishable. Three dimensional layer-by-layer growth of Ni-NPs has been observed through the whole structural analysis. As can be seen in the Fig. 5e, the grain growth follows a quasi-lateral isotropic expansion of a terrace until one side reaches the crystal edge and a preferential growth along the edge of the (1 1 1) top surface. This sequence ends when the terraces have joined all six edges of 3D superstructure.

On the basis of the above results and discussions, the formation and evolution of Ni-NPs could be described as follows: Primary nickel particles gradually were formed during sonochemical synthesis. In general Ni-NPs exhibit spherical shape, but can be seen in some particles. The dipole–dipole coupling and van der Walls attractions favor the self-organization in linear chain which can be curved due to Brownian motion. In the absence of an external magnetic field, the Ni-NPs are free to rotate and form a metastable arrangement, phenomenon known as magnetic frustration. Furthermore, the slow formation of branched chains was elucidated as a cooperative effect of the magnetic interaction between Ni-NPs. Finally, the self-organization in 2D and 3D are formed due to stacking of monolayers and grain growth of terraces.

4. Conclusions

In summary, nickel nanoparticles with controllable size and morphology can be easily obtained through a sonochemical synthesis in a PVP-assisted reaction system. The Ni-NPs evolve from a nanometric like-spherical morphology to 3D superstructures. Specifically, the growth mechanism for, 2D and 3D superstructure, involved the stacking and extension of terraces. These results represent a straightforward pathway for tuning the magnetic properties of nickel nanoparticles by controlling the self-organization as a function of time.

Declaration of interest statement

The authors declare no competing financial interest

Acknowledgments

The authors are grateful to the Instituto Mexicano del Petroleo and Laboratorio de microscopia de ultra alta resolución for assistance in TEM/HRTEM/SEM. IHP, LDBA, VGF, RSP, PS and LGR thank to the SNI for the distinction of their membership.

References

[1] Meital Shviro, David Zitoun, Nickel nanocrystals: fast synthesis of cubes, pyramids and tetrapods, RCS Adv. 3 (2013) 1380–1387.
[2] T.M. Whitney, P.C. Searson, J.S. Jiang, C.L. Chien, Fabrication and magnetic properties of arrays of metallic nanowires, Science 261 (1993) 1316–1319.
[3] G. Eldon, Emberly, George Kirczenow, Molecular spintronics: spin-dependent electron transport in molecular wires, Chem. Phys. 281 (2002) 311–324.
[4] Yao Li, Bin Ma, Jiupeng Zhao, Wuhong Xin, Xianjie Wang, Excellent mechanical properties of three-dimensionally ordered macroporous nickel photonic crystals, J. Alloys Compd. 509 (2011) 290–293.
[5] Clemens Burda, Xiaobo Chen, Radha Narayanan, Mostafa A. El-Sayed, Chemistry and properties of nanocrystals of different shapes, Chem. Rev. 105 (2005) 1025–1102.
[6] C.B. Murray, C.R. Kagan, M.G. Bawendi, Self-Organization of CdSe nanocrystallites into three-dimensional quantum dot superlattices, Science 270 (1995) 1335–1338.
[7] D.V. Talapin, E.V. Shevchenko, C.B. Murray, A.V. Titov, P. Král, Dipole–Dipole interactions in nanoparticle superlattices, Nano Lett. 7 (2007) 1213–1219.
[8] T. Oonishi, S. Sato, H. Yao, K. Kimura, Three-dimensional gold nanoparticle superlattices: structures and optical absorption characteristics, J. Appl. Phys. 101 (2007), 114314 – 114314-5.
[9] S.I. Stoeva, B.L.V. Prasad, S. Uma, P.K. Stoimenov, V. Zaikovski, C.M. Sorensen, K.J. Klabunde, Face-Centered Cubic and hexagonal closed-packed nanocrystal superlattices of gold nanoparticles prepared by different methods, J. Phys. Chem. B 107 (2003) 7441–7448.
[10] S.I. Stoeva, B.L.V. Prasad, S. Uma, P.K. Stoimenov, V. Zaikovski, C.M. Sorensen, K.J. Klabunde, Crystal structures of molecular gold nanocrystal arrays, J. Phys. Chem. B 107 (2003) 7441–7448.
[11] B.A. Korgel, S. Fullam, S. Connolly, D. Fitzmaurice, Assembly and self-organization of silver nanocrystal superlattices: ordered "soft spheres", J. Phys. Chem. B 102 (1998) 8379–8388.
[12] S.A. Harfenist, Z.L. Wang, M.M. Alvarez, I. Vezmar, R.L. Whetten, Highly oriented molecular Ag nanocrystal arrays, J. Phys. Chem. 100 (1996) 13904–13910.
[13] S.A. Harfenist, Z.L. Wang, R.L. Whetten, I. Vezmar, M.M. Alvarez, Three-dimensional hexagonal close-packed superlattice of passivated Ag nanocrystals, Adv. Mater. 9 (1997) 817–822.
[14] I. Lisiecki, P.A. Albouy, M.P. Pileni, Face-Centered-Cubic "Supracrystals" of cobalt nanocrystals, Adv. Mater. 15 (2003) 712–716.
[15] I. Lisiecki, D. Parker, C. Salzemann, M.P. Pileni, Face-Centered Cubic supra-crystals and disordered three-dimensional assemblies of 7.5 nm cobalt nanocrystals: influence of the mesoscopic ordering on the magnetic properties, Chem. Mater. 19 (2007) 4030–4036.
[16] D.S. Sidhaye, T. Bala, S. Srinath, H. Srikanth, P. Poddar, M. Sastry, B.L.V. Prasad, Preparation of nearly monodisperse nickel nanoparticles by a facile solution based methodology and their ordered assemblies, J. Phys. Chem. C 113 (2009) 3426–3429.
[17] H.L. Niu, Q.W. Chen, M. Ning, Y.S. Jia, X.J. Wang, Synthesis and one-dimensional self-assembly of acicular nickel nanocrystallites under magnetic fields, J. Phys. Chem. B 108 (2004) 3996–3999.
[18] W. Zhou, L. He, R. Cheng, L. Guo, C. Chen, J. Wang, Synthesis of Ni nanochains with various sizes: the magnetic and catalytic properties, J. Phys. Chem. C 113 (2009) 17355–17358.
[19] Z.P. Liu, S. Li, Y. Yang, S. Peng, Z.K. Hu, Y.T. Qian, Complex-surfactant-assisted hydrothermal route to ferromagnetic nickel nanobelts, Adv. Mater. 15 (2003) 1946–1948.
[20] Q. Wang, B. Geng, S. Wang, J. Liu, Z. Cheng, D. Si, A facile sonochemical route to morphology controlled nickel complex mesostructures, CrystEngComm 11 (2009) 1317–1322.
[21] Y. Li, Y. Cao, D. Jia, A general strategy for synthesis of metal nanoparticles by a solid-state redox route under ambient conditions, J. Mater. Chem. A 2 (2014) 3761–3765.
[22] T.H. Vo, U.G.E. Perera, M. Shekhirev, M.M. Pour, D.A. Kunkel, H. Lu, A. Gruverman, E. Sutter, M. Cotlet, D. Nykypanchuk, P. Zahl, A. Enders, A. Sinitskii, P. Sutter, Nitrogen-doping induced self-assembly of graphene nanoribbon-based two-dimensional and three-dimensional metamaterials, Nano Lett. 15 (2015) 5770–5777.
[23] S. Li, X. Huang, H. Li, H. Cai, C.L. Gan, F. Boey, H. Zhang, Surface-induced synthesis and self-assembly of metal suprastructures, Small 6 (2010) 2708–2715.
[24] B.D. Cullity, S.R. Stock, Elements of X-ray diffraction, Prentice Hall, NJ, USA, 2001, pp. 385–433.
[25] I. Hernández-Perez, A.M. Maubert, Luis Rendón, Patricia Santiago, H. Herrera-Hernández, L. Díaz-Barriga Arceo, V. Garibay Febles, Eduardo Palacios González, L. González-Reyes, Ultrasonic synthesis: structural, optical and electrical correlation of TiO_2 nanoparticles, Int. J. Electrochem. Sci. 7 (2012) 8832–8847.
[26] N.R. Nik Roselina, A. Azizanb, Ni nanoparticles: study of particles formation and agglomeration, Procedia Eng. 41 (2012) 1620–1626.
[27] W. Chen, A. Bian, A. Agarwal, L.Q. Liu, H.B. Shen, L.B. Wang, C.L. Xu, N.A. Kotov, Nanoparticle superstructures made by polymerase chain reaction: collective interactions of nanoparticles and a new principle for chiral materials, Nano Lett. 9 (2009) 2153–2159.
[28] S. Blundell, Small Magnetic Particles, Domains in magnetism in condensed Matter, Oxford Master Series in Condensed Matter Physics, Oxford Univ. Press Inc., New York, 2001, pp. 128–129.
[29] Z.L. Schaefer, K.M. Weeber, R. Misra, P. Schiffer, R.E. Schaak, Bridging hcp-Ni and Ni_3C via a Ni_3C_{1-x} solid solution: tunable composition and magnetism in colloidal nickel carbide nanoparticles, Chem. Mater. 23 (2011) 2475–2480.

[30] M.R. Vaezi, M.B. Vishlaghi, M.F. Tabriz, O.M. Moradi, Effect of experimental factors on magnetic properties of nickel nanoparticles produced by chemical reduction method using a statistical design, J. Alloys Compd. 623 (2015) 118–123.
[31] D. Maity, Md.M.R. Mollick, D. Mondal, B. Bhowmick, N.S. Kumar, A. Banerjee, S. Chattopadhyay, S. Bandyopadhyay, D. Chattopadhyay, Synthesis of HPMC stabilized nickel nanoparticles and investigation of their magnetic and catalytic properties, Carbohyd. Polym. 98 (2013) 80–88.
[32] G. Zhang, L. Zhao, Study on the morphologies of nickel crystals and their magnetic properties, Mater. Lett. 79 (2012) 142–144.
[33] K.P. Donegan, J.F. Godsell, D.J. Otway, M.A. Moriss, S. Roy, J.D. Holmes, Size tuneable synthesis of nickel nanoparticles, J. Nanopart. Res. 4 (2012) 1–10.
[34] C. Gatel, F.J. Bonilla, A. Meffre, E. Snoeck, B. Warot-Fonrose, B. Chaudret, L.M. Lacroix, T. Blond, Size specific spin configurations in single iron nanomagnet from flower to exotic vortices, Nano Lett. 15 (2015) 6952–6977.
[35] Robert C. O'Handley, Modern Magnetic Materials, Magnetic anisotropy, John Willey and Sons, New York, 1999, pp. 179–213.
[36] J. Townsend, R. Burtovyy, Y. Galabura, I. Luzinov, Flexible chains of ferromagnetic Nanoparticles, ACS Nano 8 (2014) 6970–6978.